Chapter 1
Laser-Assisted Electron Scattering and Diffraction in Ultrashort Intense Laser Fields

Reika Kanya, Yuya Morimoto, and Kaoru Yamanouchi

Abstract Recent progress in experimental studies of laser-assisted electron scattering (LAES) in ultrashort intense laser fields is reviewed. After a brief survey of theoretical backgrounds of the LAES process and earlier LAES experiments started in 1970's, new phenomena induced by LAES experiments in ultrashort intense laser fields and expected applications of these experiments are discussed. A new experimental setup designed for measurements of LAES induced by ultrashort intense laser fields is described. Experimental results of energy spectra, angular distributions, and laser polarization dependence of the LAES signals are presented with corresponding results of numerical simulations. A light-dressing effect appearing in the LAES signals to be obtained under our experimental conditions is also examined by numerical calculations. In addition, as an application of the LAES process, the determination of instantaneous geometrical structure of molecules by a novel technique of laser-assisted electron diffraction is introduced.

1.1 Introduction

1.1.1 Electron-Atom Collisions in Laser Fields

Through elastic scattering process between an electron and an atom occurring in a laser field, the kinetic energy of the scattered electron (E_f) can be shifted by multiples of photon energy ($\hbar\omega$), i.e., $E_f = E_i + n\hbar\omega$, where E_i is the initial kinetic energy and $n = 0, \pm1, \pm2, \ldots$. This process is called "laser-assisted electron scattering (LAES)" or "free-free transition." In some cases, the energy gain process ($n > 0$)

R. Kanya (✉) · Y. Morimoto · K. Yamanouchi
Department of Chemistry, School of Science, the University of Tokyo, 7-3-1 Hongo, Bunkyo-ku, Tokyo 113-0033, Japan
e-mail: kanya@chem.s.u-tokyo.ac.jp

Y. Morimoto
e-mail: morimoto@chem.s.u-tokyo.ac.jp

K. Yamanouchi
e-mail: kaoru@chem.s.u-tokyo.ac.jp

K. Yamanouchi et al. (eds.), *Progress in Ultrafast Intense Laser Science X*,
Springer Series in Chemical Physics 106, DOI 10.1007/978-3-319-00521-8_1,

and energy loss ($n < 0$) process are separately called "inverse bremsstrahlung" and "stimulated bremsstahlung," respectively, referring to the bremsstrahlung, which is the light emission induced by a sudden acceleration of incident electrons by an atomic potential. As an elementary process in astronomy, plasma physics, and intense laser physics, the LAES plays important roles in the infrared opacity of the solar atmosphere, the plasma heating, and the laser-induced rescattering in intense laser fields. The LAES process can also be regarded as a special kind of three-body collision, where a laser photon acts as a simple third-body in the electron-atom collision process.

Such energy gain and loss of scattered electrons by $n\hbar\omega$ can also be induced through "inelastic" scattering processes, which are called simultaneous electron-photon excitation (SEPE) or laser-assisted electron inelastic scattering in a similar manner as in the LAES process. Especially, the energy gain and loss by $n\hbar\omega$ associated with electron impact ionizations are called "laser-assisted electron impact ionization" or "laser-assisted $(e, 2e)$" processes. Experimental and theoretical studies on these inelastic phenomena were reviewed by Mason [1].

1.1.2 Theory of the LAES Process

Theoretical framework of the LAES process was proposed first by Bunkin and Fedorov in 1966 [2]. Under the first Born approximation for the scattering process between a target atom and an electron expressed as an eigenfunction of a free electron in an electromagnetic field, i.e., Gordon-Volkov wavefunction [3, 4], they derived the differential cross section for net n-photon absorption, $d\sigma^{(n)}_{\mathrm{BFA}}/d\Omega$, as

$$\frac{d\sigma^{(n)}_{\mathrm{BFA}}}{d\Omega} = \frac{|\boldsymbol{p}_f|}{|\boldsymbol{p}_i|} J_n^2(\boldsymbol{\alpha}_0 \cdot \boldsymbol{s}) \frac{d\sigma_{\mathrm{FBA}}(\boldsymbol{s})}{d\Omega}, \tag{1.1}$$

where $J_n(x)$ is the n-th order Bessel function of the first kind, $\boldsymbol{p}_i$ and $\boldsymbol{p}_f$ are initial and final electron momenta, respectively, $d\sigma_{\mathrm{FBA}}(\boldsymbol{s})/d\Omega$ is a differential cross section of elastic scattering without laser fields derived by the first Born approximation, $\boldsymbol{s}$ is a scattering vector defined by $(\boldsymbol{p}_i - \boldsymbol{p}_f)/\hbar$, and $\boldsymbol{\alpha}_0$ is defined as

$$\boldsymbol{\alpha}_0 \equiv \frac{e}{m\omega^2}\boldsymbol{\varepsilon}, \tag{1.2}$$

where e is unit charge, m is mass of an electron, and $\boldsymbol{\varepsilon}$ is an electric amplitude vector of the laser field. The absolute value of $\boldsymbol{\alpha}_0$, $|\boldsymbol{\alpha}_0|$, corresponds to the quiver radius, i.e., the amplitude of the classical motion of an electron in the electromagnetic field. In the Bunkin-Fedorov approximation (BFA), the interaction between an atom and a laser field is neglected, and the electron-atom interaction is treated within the first Born approximation, which is a good approximation for the forward scattering of high-energy electrons, and the non-perturbative interaction between an electron and a laser field is explicitly treated by using the Gordon-Volkov wavefunctions for the incident and scattered electrons. Equation (1.1) shows that the differential cross section for the $n = 0$ LAES process is also modified by the laser field. Because the

scattered electrons of this $n = 0$ LAES process have an overlap in the kinetic energy with the electrons scattered by an elastic scattering process without laser fields, the scattering processes in which $E_i = E_f$ is satisfied are referred to commonly as "$n = 0$ scattering" in the present paper.

In 1973, Kroll and Watson derived the differential cross section of LAES process by taking into account the non-perturbative interaction between an electron and an atom [5]. In the Kroll-Watson approximation (KWA), the formula of the differential cross section for net n-photon absorption, $d\sigma^{(n)}_{\mathrm{KWA}}/d\Omega$, takes a similar form to (1.1), and is written as

$$\frac{d\sigma^{(n)}_{\mathrm{KWA}}}{d\Omega} = \frac{|\boldsymbol{p}_f|}{|\boldsymbol{p}_i|} J_n^2(\boldsymbol{\alpha}_0 \cdot \boldsymbol{s}) \frac{d\sigma_{\mathrm{el}}(\tilde{E}_i; \boldsymbol{s})}{d\Omega}, \tag{1.3}$$

where $d\sigma_{\mathrm{el}}(\tilde{E}_i; \boldsymbol{s})/d\Omega$ is the differential cross section of elastic electron scattering, $\tilde{\boldsymbol{p}}_i - \hbar \boldsymbol{s} \leftarrow \tilde{\boldsymbol{p}}_i$, occurring without laser fields with an incident electron whose initial momentum, $\tilde{\boldsymbol{p}}_i$, and initial kinetic energy, $\tilde{E}_i$, are defined as

$$\tilde{\boldsymbol{p}}_i \equiv \boldsymbol{p}_i + \frac{nm\omega}{(\boldsymbol{\alpha}_0 \cdot \boldsymbol{s})} \boldsymbol{\alpha}_0, \tag{1.4}$$

$$\tilde{E}_i \equiv \frac{|\tilde{\boldsymbol{p}}_i|^2}{2m}, \tag{1.5}$$

respectively. Equation (1.3) means that the differential cross section of the LAES process is calculated from $d\sigma_{\mathrm{el}}(E_i; \boldsymbol{s})/d\Omega$, which can be given by conventional scattering experiments without a laser field, or obtained from a database provided, for example, by NIST [6]. The Kroll-Watson formula can also be applied to the slow-electron scattering and the backward scattering. However, the formation of light-dressed states of target atoms could not be described because the interaction between an atom and a laser field is neglected.

Mittleman et al. [7–10] developed a theoretical framework for an electron-atom scattering in the presence of a laser field whose frequency is near resonant to the atomic transition. Zon [11, 12] proposed a simple and convenient model by describing the laser-atom interaction as the polarization of electron clouds of target atoms induced by the off-resonant laser fields. Later, Byron et al. [13, 14] studied the effect of the formation of light-dressed atoms by treating the laser-atom interaction by a first-order time-dependent perturbation theory and the electron-atom interaction by the first Born approximation. Non-perturbative interactions between laser fields and atoms in high-energy electron-atom scattering processes can be treated in Born-Floquet theory proposed by Faisal [15], or non-Hermitian Born-Floquet theory developed by Dörr et al. [16], while R-matrix Floquet theory [17, 18] and close-coupling Floquet theory [19] are applicable for low-energy scattering process, in which the non-perturbative electron-atom interaction is included in addition to the non-perturbative laser-atom interaction. In addition, other theoretical methods were also proposed on the basis of a variety of models and approximations as reviewed in [20].

1.1.3 Experimental Studies of the LAES

The first observation of LAES was reported by Andrick and Langhans in 1976 [21], who observed $n = \pm 1$ LAES signals in the electron-Ar collision process under a continuous laser filed ($\lambda = 10.6$ μm, $I = 6 \times 10^4$ W/cm^2) generated by cw-CO_2 laser. In the next year, Weingartshofer et al. reported multiphoton-LAES signals up to $n = \pm 3$ in the electron-Ar scattering with a pulsed-CO_2 laser ($\lambda = 10.6$ μm, $I = 10^9$ W/cm^2, $\Delta t = 2$ μs) [22]. Compared to the theoretical studies, only a small number of experimental studies [1, 23] have been reported probably because LAES measurements are very difficult. Until 2010, the kinetic energies of an incident electron beam in LAES experiments had been in the low energy range, 4 eV $< E_i <$ 80 eV, and all the laser light sources were cw-CO_2 lasers [21, 24–27] or pulsed-CO_2 lasers with the minimum pulse duration of the order of microseconds [22, 28–38], except a study with cw-CO laser ($I = 10^3$ W/cm^2, $\lambda = 5.3$ μm) [39]. Consequently, in these experimental studies, the laser field intensities were in the rather moderate range ($<10^9$ W/cm^2) and the photon energies were too small to induce electronic transitions of target atoms. Therefore, no evidences of the formation of the light-dressed states of target atoms were identified in these traditional LAES experiments, as concluded by several theoretical estimations [40–42].

Interestingly, in 1970's, Hertel et al. reported their results of laser-induced superelastic scattering experiments, i.e., the electron scattering experiments in which target atoms are resonantly excited by cw-laser fields [43, 44]. These experiments are regarded as electron scattering by light-dressed atoms occurring when the laser-electron interaction is negligibly small. This is the opposite situation to the conventional LAES experiments, in which light-dressed electrons are scattered by non-dressed target atoms. So far, no experimental report has been made on "scattering of light-dressed electrons by light-dressed atoms."

1.1.4 LAES Experiment in Femtosecond Intense Laser Fields

In 2010, we observed LAES signals induced by femtosecond near-infrared intense laser fields ($I = 1.8 \times 10^{12}$ W/cm^2, $\lambda = 800$ nm, $\Delta t = 200$ fs) in the elastic scattering of 1 keV electrons by Xe atoms [45]. This is the first observation of LAES by femtosecond laser pulses. Compared to the conventional LAES experiments, such as the latest LAES experiment with a pulsed-CO_2 laser ($I = 4 \times 10^8$ W/cm^2, $\lambda = 10.6$ μm, $\Delta t = 3$ μs, $E_i = 22$ eV) [38], the experimental conditions in our study [45] were completely different in the following four points; (i) the photon energy is 13 times higher, (ii) the laser intensity is 4.5×10^3 times higher, (iii) the laser pulse duration is 1.5×10^7 times shorter, and (iv) the kinetic energy of the incident electrons is 45 times larger than the latest conventional LAES study [38].

The large differences in the photon energy and the laser intensity will enable us to perform experiments on LAES by light-dressed atoms. Several theoretical studies

predicted that a peak structure will appear at the zero scattering angle in the angular distributions of LAES signals when target atoms form light-dressed electronic states [11, 13], and the intensity of the peak appearing in the small scattering angle region increases drastically when a substantial electronic-state mixing occurs through resonant interactions between laser fields and atoms [16, 18, 19]. Therefore, LAES occurring in intense near-infrared laser fields should carry information on light-dressed states of target atoms having ultrashort lifetimes in intense laser fields. On the other hand, ultrashort laser pulses for LAES experiments enable us to achieve high temporal resolutions, and LAES by molecules with high-energy electrons can carry information on geometrical structure of molecules as in electron diffraction of gas-phase molecules. This means that LAES by molecules will lead to "a new time-resolved electron diffraction method" with the temporal resolution of femtoseconds [45].

After the first observation of the LAES signals induced by 200 fs laser pulses [45], a LAES experiment with 50 fs laser pulses was reported in 2011 also by our group [46], and another near-infrared LAES experiment was reported in 2011 by deHarak et al., where Nd:YAG laser ($\Delta t = 6$ ns, $\lambda = 1064$ nm) was used for generating laser fields of the order of 10^9 W/cm^2 [47]. It can be said that experimental studies of the LAES process are now entering into a new stage 34 years after the first conventional LAES experiment [21].

In the present article, the recent progress of the LAES experiments in femtosecond intense laser fields is reviewed, and promising applications of LAES processes to "probing of light-dressed states" and "gas electron diffraction" are discussed by referring to our numerical simulations.

1.2 Experimental Setup

Details of the experimental setup were described in [46]. Figure 1.1 shows the schematic of our setup for femtosecond-LAES experiments. The apparatus consists of a femtosecond laser system, an electron beam source, a sample gas nozzle, a toroidal-type electron energy analyzer, and an imaging detector. Scattered electrons generated by the collision among the three beams, i.e., the electron beam, the atom beam, and the laser beam, are introduced into the electron energy analyzer and are detected by the imaging detector.

By taking the leading term of the Bessel functions in (1.1) or (1.3), intensities of the LAES signals in BFA and KWA are approximately proportional to $\Delta t(\lambda^4 I)^{|n|}$. This means that the signal intensities per laser-shot for the $n = \pm 1$ transitions in LAES should decrease by a factor of 1×10^{-8} when the laser field conditions change from "$\Delta t = 3$ μs, $\lambda = 10.6$ μm, $I = 4 \times 10^8$ W/cm^2" to "$\Delta t = 200$ fs, $\lambda = 800$ nm, $I = 1.8 \times 10^{12}$ W/cm^2," which correspond to the conditions employed in the latest conventional LAES experiment with CO_2 laser [38] and our first femtosecond-LAES experiment [45], respectively. Therefore, a drastic improvement in the detection efficiency is necessary for the measurements of the LAES signals

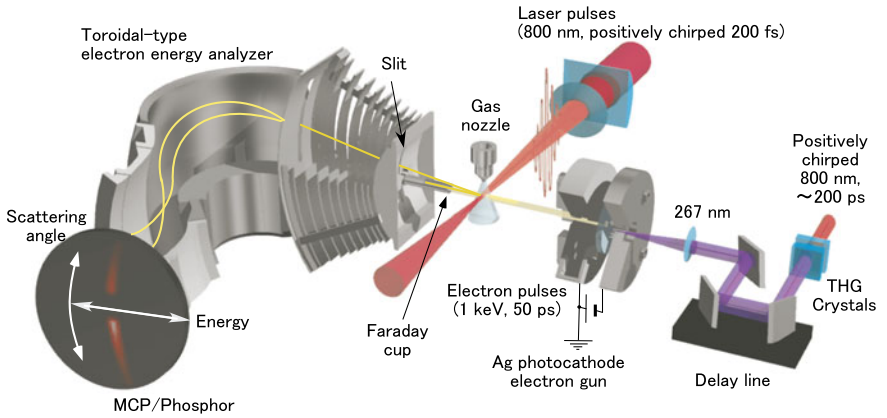

Fig. 1.1 The schematic of the experimental setup of LAES [46]

in ultrashort intense laser fields. Furthermore, because of the limited spatial overlap and the velocity mismatch between the electron pulse and the femtosecond laser pulse [48], the fraction of scattering events in the laser field is estimated to be only 0.4 %, and majority of the scattering events (99.6 %) are those occurring in the absence of the laser fields under the experimental conditions, in which a pulsed 1 keV electron beam collides with a sample gas beam of ~1 mm diameter at right angles and a 200 fs laser pulse is introduced perpendicularly to both the electron and sample beams. Thus, it is difficult to discriminate the femtosecond-LAES signals in the energy spectra of the scattered electrons from the neighboring huge peak of $n = 0$ scattering signals. Moreover, intensities of the LAES signals will be similar in magnitude to noise signals originating from stray photons, photoelectrons, photoions, and metastable neutral atoms generated by the irradiation of intense near-infrared laser pulses. In order to overcome the experimental difficulties mentioned above, the following three components are newly introduced into our LAES apparatus, i.e., (i) the electron beam source with a photocathode-type pulsed electron gun, (ii) the high repetition-rate and high power Ti:sapphire laser system, and (iii) the toroidal-type electron energy analyzer equipped with the two-dimensional detector.

The electron pulses are generated from the photocathode-type pulsed electron gun by irradiating the photocathode with UV laser pulses, which are the third harmonics of 800 nm light split from the main 800 nm pulses before a pulse compressor of the laser system. The synchronization between the electron pulse and the intense IR laser pulse for the LAES process is achieved by adjusting the optical delay between the UV laser pulses and the intense IR laser pulses. The pulse duration of the electron pulses were found to be ~50 ps by the shadow graph method [46]. Huge background signals originating from elastic scattering without laser fields can be suppressed by using these ultrashort incident electron pulses. The generated monochromatic electron pulse of 1 keV kinetic energy collides with a Xe gas in a near-infrared intense laser field ($\Delta t = 200$ fs, $\lambda = 800$ nm, $I = 1.8 \times 10^{12}$ W/cm^2) at the scattering point in the vacuum chamber. The scattered electrons are introduced

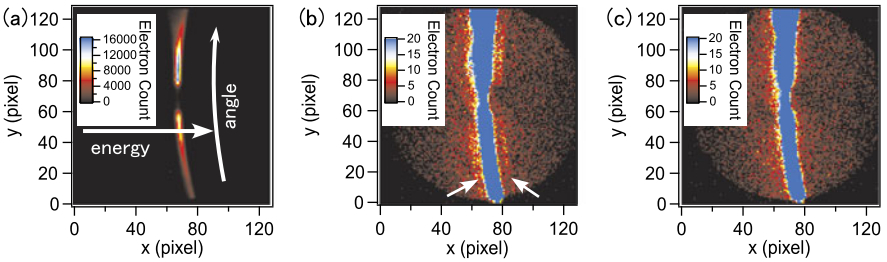

Fig. 1.2 (**a**) The raw image of electron scattering signals recorded when vertically polarized laser pulses were introduced at the timing of the electron scattering by Xe atoms. (**b**) The amplified image of (**a**). (**c**) The raw image of background signals in the same intensity scale as (**b**) [45]

into the toroidal-type electron energy analyzer through a 0.8 mm slit. Simultaneous detection of the angular and energy distributions is achieved by the toroidal-type electron energy analyzer [49], and these distributions are obtained as a two-dimensional image on a MCP/Phosphor detector coupled with a CCD camera. On the detector, an angular distribution of isoenergetic electrons forms an arcuate pattern as shown in Fig. 1.1. The signals of scattered electrons are discriminated from noise signals by counting the number of bright spots of electron signals appearing on CCD images within a time window of one second. Significant improvement in the count rate of the LAES signals is achieved by 5 kHz data acquisition with the high repetition-rate and high power Ti:sapphire laser system. The number of incident electrons per shot is made as small as possible in order to avoid energy broadening induced by the space charge effect, and a typical count rates of detection of electrons including those originating from the elastic scattering is around 10 cps. The energy resolution of the total detection system is around 0.7 eV, which is sufficiently smaller than the photon energy of laser light (1.56 eV).

1.3 Observation of LAES in Intense Laser Fields

The raw images of scattered electrons obtained from the LAES experiments with the light field conditions of $\Delta t = 200$ fs, $\lambda = 800$ nm, and $I = 1.8 \times 10^{12}$ W/cm^2 [45] are shown in Fig. 1.2. The net exposure time was around 83 hours for each image. Figure 1.2(a) shows electron scattering signals when laser pulses were introduced at the timing of the electron scattering by Xe atoms. The laser polarization was set to be "vertical", i.e., perpendicular to the electron beam axis. The intense signals forming an arcuate line seen at the central area in Fig. 1.2(a) is $n = 0$ scattering signals, and any other features could not be recognized in Fig. 1.2(a). Figure 1.2(b) is an amplified image of Fig. 1.2(a) obtained after adjusting the range of the signal intensity so that the weak LAES signals become visible. In Fig. 1.2(b), a weak arcuate lines indicated by the white arrows can be seen on both sides of the central arcuate line. On the other hand, such structures could not be seen in the background

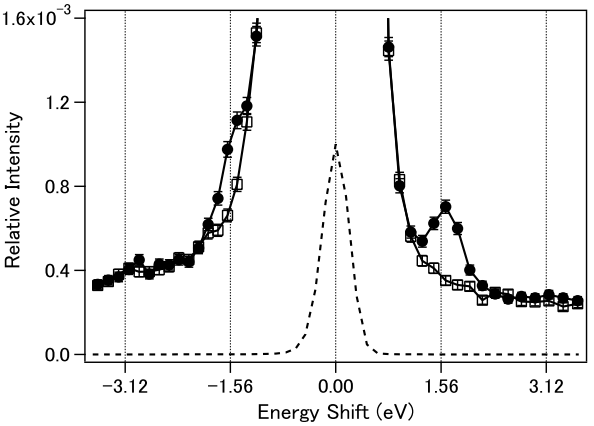

Fig. 1.3 The energy spectra of relative intensities of scattered electron signals [45]. The intensity is normalized with respect to the peak intensity of $n = 0$ scattering signal. Estimated statistical error bars are derived from square roots of signal counts. *Filled circles*: electron signals with vertically polarized laser fields; *Open squares*: background signals; *Broken line*: $n = 0$ scattering peak reduced by a factor of 1000

signals [Fig. 1.2(c)], which is obtained when the temporal delay of the electron pulse with respect to the laser pulse was set to be +100 ps.

The observed small difference between Figs. 1.2(b) and 1.2(c) becomes clear in the electron energy spectra, which are obtained through the integration of the signal of each pixel over the scattering angles along the arcuate isoenergetic coordinate. In the integration, signals in the region of $y > 105$ pixel in Fig. 1.2 were excluded from the analysis because the contributions of stray electrons are significantly large in this region. The filled circles and the open squares in Fig. 1.3 show the energy spectra obtained from Fig. 1.2(b) and (c), respectively. Unambiguous increases in the signal intensity appear at the kinetic energy shifts of $\pm\hbar\omega$, i.e., ± 1.56 eV, in Fig. 1.3 (filled circles). This is a clear experimental evidence that the $n = \pm 1$ transitions in the LAES process are identified.

The filled circles in Fig. 1.4 represent the LAES signals obtained by subtracting the background signals from the scattering signals obtained with the laser field in Fig. 1.3. Both of the signals at the energies of $\pm\hbar\omega$ can be recognized as distinct peaks, and the intensities of these peaks are around 3×10^{-4} relative to the central $n = 0$ scattering peak.

In order to confirm our assignment, the relative intensities of the LAES signals were estimated by a numerical simulation based on (1.3). In the current experimental configuration with $\hat{\boldsymbol{\varepsilon}} \cdot \boldsymbol{p}_i = 0$, the $\tilde{\boldsymbol{p}}_i$ can be expressed as

$$\tilde{\boldsymbol{p}}_i = \boldsymbol{p}_i - \frac{n\hbar\omega|\boldsymbol{p}_f|}{2E_f \sin\theta}\hat{\boldsymbol{\varepsilon}}, \tag{1.6}$$

where $E_f \equiv |\boldsymbol{p}_f|^2/(2m)$ is the kinetic energy of a scattered electron. In the present high-energy scattering ($E_f \sim 1$ keV), $|\tilde{\boldsymbol{p}}_i| \simeq |\boldsymbol{p}_i|$ holds well because $\hbar\omega/(2E_f \sin\theta)$ is less than 0.03 in the detectable range of the scattering angle (1.5 deg. $< \theta <$ 14 deg.). Then, the $d\sigma^{(n)}_{\mathrm{KWA}}/d\Omega$ can be approximated to be

$$\frac{d\sigma^{(n)}_{\mathrm{KWA}}}{d\Omega} \simeq \frac{|\boldsymbol{p}_f|}{|\boldsymbol{p}_i|} J_n^2(\boldsymbol{\alpha}_0 \cdot \boldsymbol{s}) \frac{d\sigma(E_i; \boldsymbol{s})}{d\Omega}. \tag{1.7}$$

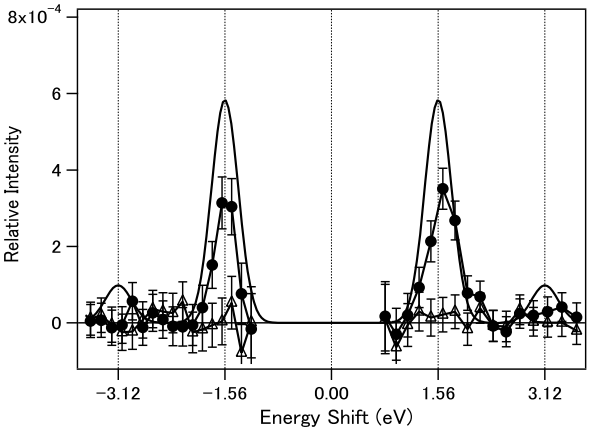

Fig. 1.4 The energy spectra of relative intensities of LAES signals [45]. Relative intensities are normalized with respect to the peak intensity of $n = 0$ scattering signal. Estimated statistical error bars are derived from square roots of signal counts. *Filled circles*: an energy spectrum obtained after the subtraction of the backgrounds from the signals recorded with vertically polarized laser fields; *Open triangles*: an energy spectrum obtained after the subtraction of the backgrounds from the signals recorded with horizontally polarized laser fields; *Solid line*: a calculated spectrum of the LAES signals when the laser fields are vertically polarized

In order to simulate the magnitudes of the observed LAES signals, denoted by $w^{(n)}(E_i; \boldsymbol{s})$, the differential cross section in (1.7) should be averaged over the spatiotemporal distribution of the three beams, i.e., the electron beam, the laser beam, and the atomic beam. Considering that the $d\sigma(E_i; \boldsymbol{s})/d\Omega$ is independent of the laser field, the $w^{(n)}(E_i; \boldsymbol{s})$ can be factorized into two parts,

$$w^{(n)}(E_i; \boldsymbol{s}) = F_n(E_i; \boldsymbol{s}) \frac{d\sigma(E_i; \boldsymbol{s})}{d\Omega}, \tag{1.8}$$

where

$$F_n(E_i; \boldsymbol{s}) \equiv \frac{|\boldsymbol{p}_f|}{|\boldsymbol{p}_i|} \int d\boldsymbol{r}\, \rho(\boldsymbol{r}) \int dt\, j(\boldsymbol{r}, t) J_n^2\big(\boldsymbol{\alpha}_0(\boldsymbol{r}, t) \cdot \boldsymbol{s}\big). \tag{1.9}$$

In (1.9), $\rho(\boldsymbol{r})$ is a density of the sample atom and $j(\boldsymbol{r}, t)$ is an electron flux density. The spatiotemporal distributions of the $\rho(\boldsymbol{r})$ and $j(\boldsymbol{r}, t)$ can be determined experimentally [46]. The vectorial quiver radius, $\boldsymbol{\alpha}_0(\boldsymbol{r}, t)$, becomes a function of $\boldsymbol{r}$ and t because of the spatiotemporal distribution of $\boldsymbol{\varepsilon}$, and can also be derived experimentally, as described in [46], using the laser field parameters, such as the pulse energy, the temporal shape of the pulse envelope, and the spatial profile at the scattering point. Therefore, $w^{(n)}(E_i; \boldsymbol{s})$ in (1.8) can be calculated using $F_n(E_i; \boldsymbol{s})$ obtained from (1.9) and the differential cross section $(d\sigma(E_i; \boldsymbol{s})/d\Omega)$ in the NIST database [6]. The results of the simulation are plotted with a solid line in Fig. 1.4. The calculated LAES signal intensities relative to $n = 0$ scattering signal intensities show good agreement with the experimental results.

When the laser polarization vector is set to be "horizontal", i.e., parallel to the direction of the incident electron beam, the factor of $\boldsymbol{\alpha}_0 \cdot \boldsymbol{s}$ in (1.3) becomes close to

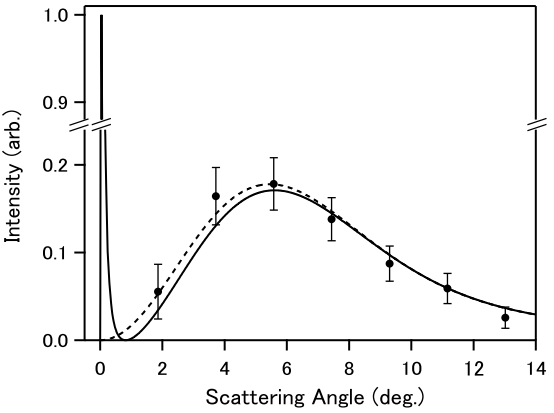

Fig. 1.5 The angular distributions of LAES for the $n = +1$ transitions with the vertically polarized laser field [45, 50]. *Filled circles*: observed LAES signals of $n = +1$; *Broken line*: the numerical calculation by KWA; *Solid line*: the numerical calculation by Zon's model. Estimated statistical error bars are derived from square roots of the signal counts

zero because the polarization vector is nearly perpendicular to the scattering vector, $\boldsymbol{s}$, for the forward scattering of the high-energy electrons. Consequently, the LAES signal intensities should be suppressed significantly except the signal intensity at $n = 0$. This polarization dependence should provide a further verification of our measurements of LAES signals of $n = \pm 1$. In Fig. 1.4, an energy spectrum with the horizontally polarized laser field is plotted with open triangles. In contrast to the corresponding spectrum obtained using the vertically polarized laser field, no distinguishable peaks are observed. This is consistent with the corresponding numerical calculation, showing that relative intensities for the $n = \pm 1$ transitions are nearly zero (7×10^{-6}).

The filled circles in Fig. 1.5 show the angular distribution of the background-subtracted LAES signals for the $n = +1$ transition recorded using the vertically polarized laser field. The broken line shows the results of numerical calculations with KWA. The calculated angular distribution is in good agreement with the experimental angular distribution. The angular distribution of the $n = -1$ transition is basically the same as that of the $n = +1$ transition, and also shows good agreement with the result of numerical calculations.

As discussed in Sect. 1.1.4, the characteristic peak structure is expected to appear at the zero angle in the angular distribution of LAES signals when target atoms are formed in the light-dressed states. This light-dressing effect [50] is examined by a simulation of the angular distribution of the $n = +1$ LAES signals using Zon's model [11] with the experimental laser field conditions ($\Delta t = 200$ fs, $\lambda = 800$ nm, $I = 1.8 \times 10^{12}$ W/cm^2). In this model, the laser-atom interaction is treated as a polarization of an electron cloud in a target atom, creating a laser-induced dipole moment expressed as

$$\boldsymbol{\mu}_{\mathrm{ind}} = a(\omega)\boldsymbol{\varepsilon} \sin \omega t, \tag{1.10}$$

where $a(\omega)$ is the frequency-dependent polarizability of the target atom, which can be described by the Unsöld expression [51] as

$$a(\omega) = a(0)\frac{\omega_{\mathrm{res}}^2}{\omega_{\mathrm{res}}^2 - \omega^2}, \tag{1.11}$$

where $\omega_{\rm res}$ is the resonance frequency of the target atom and $\omega_{\rm res} \gg \omega$ is assumed. Because the scattering process is affected by the interaction potential between the charge of the incident electron and the laser-induced dipole of the polarized atoms, the Hamiltonian of the system is expressed as

$$\hat{H} = \frac{1}{2m}\left(\frac{\hbar}{i}\nabla + m\omega\boldsymbol{\alpha}_0 \cos\omega t\right)^2 + V(\boldsymbol{r}) - \frac{e\boldsymbol{\mu}_{\rm ind}\cdot\boldsymbol{r}}{4\pi\varepsilon_0 r^3}. \tag{1.12}$$

Under the first Born approximation, the differential cross section of the LAES process can be derived analytically as

$$\frac{d\sigma^{(n)}_{\rm Zon}}{d\Omega} = \frac{|\boldsymbol{p}_f|}{|\boldsymbol{p}_i|}\left|J_n(\xi) f_{\rm Born}(\boldsymbol{s}) - \frac{m^2\omega^2 a(\omega)}{4\pi\varepsilon_0\hbar^2|\boldsymbol{s}|^2}\xi\left[J_{n-1}(\xi) - J_{n+1}(\xi)\right]\right|^2, \tag{1.13}$$

where $\xi \equiv \boldsymbol{\alpha}_0 \cdot \boldsymbol{s}$ and $f_{\rm Born}(\boldsymbol{s})$ is the scattering amplitude without laser fields expressed as

$$f_{\rm Born}(\boldsymbol{s}) = -\frac{m}{2\pi\hbar^2}\int V(\mathbf{r}) e^{i\mathbf{s}\cdot\mathbf{r}} d\mathbf{r}, \tag{1.14}$$

in the first Born approximation. The first term in the squared modulus in (1.13) represents the scattering by the non-dressed potential, $V(\boldsymbol{r})$, and the second term in the squared modulus represents the laser-induced polarization of the target atom. If the second term in (1.13) is omitted, (1.13) becomes identical to (1.1).

The solid line in Fig. 1.5 shows the result of the numerical calculation obtained with Zon's model. In the calculation, the spatiotemporal overlaps of the three beams are taken into account in the same manner as in the calculation with KWA (broken line in Fig. 1.5), and $f_{\rm Born}(\boldsymbol{s})$ is replaced by the numerical scattering amplitude given by the NIST database [6] in order to describe more accurately the scattering amplitude in the large scattering angle region. As shown with the solid curve, a sharp and intense peak profile can be seen around the zero angle region, exhibiting remarkable contrast to the calculated angular distribution shown in Fig. 1.5 with a broken line obtained by KWA. This peak profile appearing with Zon's model shows that the light dressing effect is sufficiently large in the present laser field conditions, so that the intensity of the sharp peak profile is in the detectable range. Unfortunately, the scattering signals in the small scattering-angle region could not be detected using our apparatus because the scattered electrons in the range of $\theta < 1.5$ degree are blocked by a Faraday cup placed in front of the entrance slit of the energy analyzer (Fig. 1.1).

Zon's model, in which the laser-atom interaction is considered as a perturbation, could not be used when the laser-atom interaction becomes substantially large associated with the increase in laser-field intensities. In such intense laser field conditions, Born-Floquet theory [15] and non-Hermite Born-Floquet theory [16] need to be introduced for describing LAES signals. When the laser field intensity increases more, for example, typically up to $\sim 10^{14}$ W/cm^2, even the Floquet-type theories are no longer practically feasible because the size of the Floquet Hamiltonian matrix becomes so large that a physical picture of the phenomena is difficult to be described by a Floquet-type basis set. In addition, these Floquet-type pictures hold well only

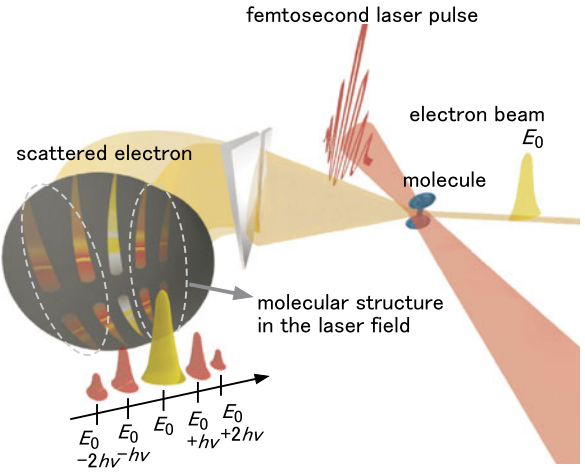

Fig. 1.6 The schematic of laser-assisted electron diffraction method

when the laser pulse duration is substantially longer than the period of the laser field, and will not hold when the laser field has only few-cycles. Therefore, another theoretical methods need to be developed to describe the LAES process induced by very intense laser pulses and/or few-cycle laser pulses.

1.4 Laser-Assisted Electron Diffraction

Gas electron diffraction has been a standard method to determine geometrical structures of molecules in the gas phase [52–54]. For probing temporal variation of geometrical structures of molecules, a pulsed gas electron diffraction method was developed, where electron diffraction patterns were obtained with ultrashort electron pulses [55]. However, the temporal resolution could not be improved beyond ∼1 ps so far [56], which is much longer than the typical timescale of nuclear motion of molecules, and, up to the present, femtosecond temporal resolution has not been achieved by the time-resolved pulsed gas electron diffraction method.

As proposed in our recent report [45], a new ultrafast gas electron diffraction method called laser-assisted electron diffraction (LAED) can be developed if the femtosecond LAES measurement is performed with a molecular target. The schematic of the LAED experiment is described in Fig. 1.6. The LAES process for molecular targets is basically the same as that for atomic targets, but interference diffraction patterns appear in the angular distribution of the LAES signals in the same manner as in conventional gas electron diffraction experiments. From the analyses of the diffraction patterns, geometrical structure of a molecule can be determined. Considering that LAES signals arise only when molecules are interacting with an ultrashort pulsed laser field, the determined geometrical structure can be regarded as “instantaneous structure” only during the femtosecond laser pulse duration. Therefore, if dynamical processes of molecules are induced by femtosecond

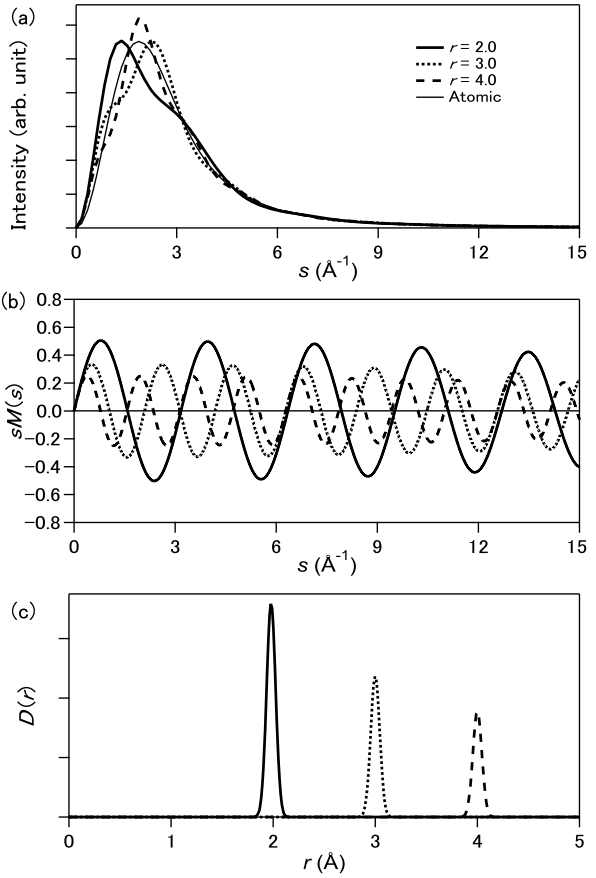

Fig. 1.7 The model calculations of (**a**) scattering intensities, (**b**) $sM(s)$, and (**c**) $D(r)$ of LAES by Cl_2 molecule with the different internuclear distances; $r = 2.0$ Å (*thick solid line*), 3.0 Å (*dotted line*), and 4.0 Å (*broken line*) for the $n = +1$ transition [45]. The mean amplitude is set to be $l_h = 0.044$ Å. Thin *solid line* in (**a**): the atomic scattering intensity of two Cl atoms

pump laser pulses and are probed by the femtosecond LAED method, the temporal resolution of the time-resolved gas electron diffraction will be of the order of femtoseconds, i.e., 10^2–10^3 times higher than ∼1 ps achieved by the previous pulsed gas electron diffraction methods [56].

The feasibility of the proposed LAED method is confirmed by the following numerical calculations. Figure 1.7(a) shows the results of numerical calculations of the scattering intensities of Cl_2 as a function of $s = |\boldsymbol{s}|$ for the $n = +1$ transition of LAES with the three different Cl-Cl internuclear distances; 2.0 Å, 3.0 Å, and 4.0 Å. In the numerical calculations, parameters describing the characteristics of the three beams and their spatiotemporal overlaps are assumed to be the same as in [45]. Through the same procedure as in the conventional gas electron diffraction method [52–54], a modified molecular scattering intensity, $sM(s)$, is obtained as shown in Fig. 1.7(b) from the observed angular distribution, and a radial distribution curve, $D(r)$, can be derived as shown in Fig. 1.7(c) through the Fourier transformation of $sM(s)$.

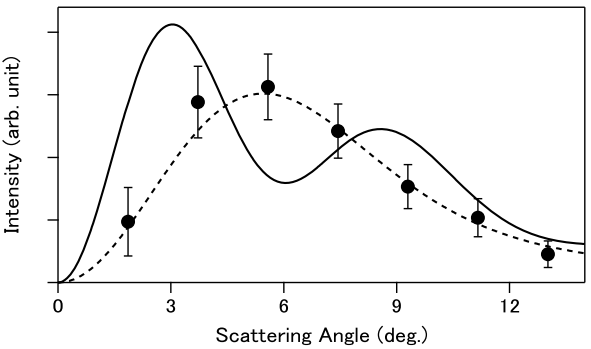

Fig. 1.8 The angular distributions of the $n = +1$ transition of LAES [57]. *Filled circles*: the observed LAES signals of Xe. *Broken line*: the calculated angular distribution of LAES signals of Xe by KWA. *Solid line*: the calculated angular distribution of LAES signals of CCl_4 by KWA

Only the additional approximation in the present procedure is KWA, which holds well for high-energy electron scattering in near-infrared laser fields as long as the dressing effect of targets is neglected. Because molecular structures are determined from the LAES signals in the relatively large scattering angle range, the light-dressing effect, that is expected to appear around the zero scattering angle ($|\boldsymbol{s}| < 0.3$ Å) as seen in Fig. 1.5, could have an only negligibly small effect in the geometrical structure of molecules to be determined. Therefore, correlation between the formation of light-dressed states and the variation of geometrical structure can be investigated by the analysis of the obtained LAED signals.

The solid line in Fig. 1.8 is a calculated angular distribution of the $n = +1$ transition of LAES by CCl_4, where the sample gas density and laser field conditions are assumed to be the same as those in the experiment of Xe [45]. The modulated interference pattern appears in the calculated angular distribution of LAES signals of CCl_4. The comparison between the modulation amplitude in the calculated LAED diffraction pattern of CCl_4 (solid line) and the observed LAES angular distribution of Xe (filled circles with the error bars) shows that the LAED method is applicable to determine geometrical structure of CCl_4. If pump-and-probe experiments are performed, the temporal evolution of the geometrical structure of CCl_4 can be probed by LAED. Therefore, the LAED method will be a promising approach for recording "molecular movies" with femtosecond temporal resolutions.

1.5 Concluding Remarks

In the present paper, recent studies of the LAES experiment in intense laser fields have been reviewed. As possible applications, "probing of light-dressed states in intense laser fields" and "laser-assisted electron diffraction with femtosecond temporal resolution" have been introduced. Considering the recent rapid advances in the technologies of high power and high repetition-rate femtosecond lasers [58–61], the count rate of LAES signals is expected to be raised by several orders of magnitude in the near future.

These experimental techniques of the femtosecond-LAES measurements can also be applied to investigations of other types of laser-assisted phenomena

associated with electron inelastic scattering processes. For example, a variety of phenomena originating from electron impact processes occurring in intense laser fields will be used for the investigation of light-dressing effects in electronically-excited states of target atoms and molecules and for developing new time-resolved spectroscopy with femtosecond temporal resolution such as time-resolved electron energy-loss spectroscopy and time-resolved laser-assisted electron momentum spectroscopy [62]. This means that the present femtosecond LAES and femtosecond LAED experiments will guide us to a new class of research themes of electron-atom collision and electron-molecule collision processes in ultrashort intense laser fields.

Acknowledgements The research was supported by the Grant-in-Aid for Specially Promoted Research (Grant No. 19002006), the Grand-in-Aid for Scientific Research (A) (Grant No. 24245003), the Grant-in-Aid for Young Scientists (B) (Grant Nos. 19750003, 24750011), Global COE Program (Chemistry Innovation through Cooperation of Science and Engineering), and Special Coordination Funds for Promoting Science and Technology, from Ministry of Education, Culture, Sports, Science and Technology (MEXT), Japan.

References

1. N.J. Mason, Rep. Prog. Phys. **56**, 1275 (1993)
2. F.V. Bunkin, M.V. Fedorov, Sov. Phys. JETP **22**, 844 (1966)
3. W. Gordon, Z. Phys. **40**, 117 (1926)
4. D.M. Volkov, Z. Phys. **94**, 250 (1935)
5. N.M. Kroll, K.M. Watson, Phys. Rev. A **8**, 804 (1973)
6. A. Jablonski, F. Salvat, C.J. Powell, *NIST Electron Elastic-Scattering Cross-Section Database—Version 3.0* (National Institute of Standards and Technology, 2002)
7. J.I. Gersten, M.H. Mittleman, Phys. Rev. A **13**, 123 (1976)
8. M.H. Mittleman, Phys. Rev. A **14**, 1338 (1976)
9. M.H. Mittleman, Phys. Rev. A **16**, 1549 (1977)
10. M.H. Mittleman, Phys. Rev. A **18**, 685 (1978)
11. B.A. Zon, Sov. Phys. JETP **46**, 65 (1977)
12. E.L. Beilin, B.A. Zon, J. Phys. B **16**, L159 (1983)
13. F.W. Byron-Jr Jr., C.J. Joachain, J. Phys. B **17**, L295 (1984)
14. F.W. Byron-Jr, P. Francken, C.J. Joachain, J. Phys. B **20**, 5487 (1987)
15. F.H.M. Faisal, *Theory of Multiphoton Processes* (Plenum, New York, 1987). Chap. 12.3.4
16. M. Dörr, C.J. Joachain, R.M. Potvliege, S. Vučić, Phys. Rev. A **49**, 4852 (1994)
17. P.G. Burke, P. Francken, C.J. Joachain, J. Phys. B **24**, 761 (1991)
18. M. Terao-Dunseath, K.M. Dunseath, J. Phys. B **35**, 125 (2002)
19. A. Cionga, L. Dimou, F.H.M. Faisal, J. Phys. B **30**, L361 (1997)
20. F. Ehlotzky, A. Jaroń, J.Z. Kamiński, Phys. Rep. **297**, 63 (1998)
21. D. Andrick, L. Langhans, J. Phys. B **9**, L459 (1976)
22. A. Weingartshofer, J.K. Holmes, G. Caudle, E.M. Clarke, H. Krüger, Phys. Rev. Lett. **39**, 269 (1977)
23. A. Weingartshofer, C. Jung, in *Multiphoton Ionization of Atoms*, ed. by S.L. Chin, P. Lambropoulos (Academic Press, New York, 1984), p. 155
24. D. Andrick, L. Langhans, J. Phys. B **11**, 2355 (1978)
25. L. Langhans, J. Phys. B **11**, 2361 (1978)
26. D. Andrick, H. Bader, J. Phys. B **17**, 4549 (1984)
27. H. Bader, J. Phys. B **19**, 2177 (1986)
28. A. Weingartshofer, E.M. Clarke, J.K. Holmes, C. Jung, Phys. Rev. A **19**, 2371 (1979)

29. A. Weingartshofer, J.K. Holmes, J. Sabbagh, S.L. Chin, J. Phys. B **16**, 1805 (1983)
30. B. Wallbank, V.W. Connors, J.K. Holmes, A. Weingartshofer, J. Phys. B **20**, L833 (1987)
31. B. Wallbank, J.K. Holmes, A. Weingartshofer, J. Phys. B **20**, 6121 (1987)
32. B. Wallbank, J.K. Holmes, S.C. MacIsaac, A. Weingartshofer, J. Phys. B **25**, 1265 (1992)
33. B. Wallbank, J.K. Holmes, Phys. Rev. A **48**, R2515 (1993)
34. B. Wallbank, J.K. Holmes, J. Phys. B **27**, 1221 (1994)
35. B. Wallbank, J.K. Holmes, J. Phys. B **27**, 5405 (1994)
36. B. Wallbank, J.K. Holmes, J. Phys. B **29**, 5881 (1996)
37. B. Wallbank, J.K. Holmes, Can. J. Phys. **79**, 1237 (2001)
38. D. Nehari, J. Holmes, K.M. Dunseath, M. Terao-Dunseath, J. Phys. B **43**, 025203 (2010)
39. H. Bader, J. Phys. B **18**, 235 (1985)
40. I. Rabadán, L. Méndez, A.S. Dickinson, J. Phys. B **27**, L535 (1994)
41. S. Geltman, Phys. Rev. A **51**, R34 (1995)
42. S. Varró, F. Ehlotzky, Phys. Lett. A **203**, 203 (1995)
43. I.V. Hertel, W. Stoll, in *Proc. Int. Conf. Phys. Electron. At. Coll., 7th* (1973), p. 321
44. I.V. Hertel, W. Stoll, Adv. At. Mol. Phys. **13**, 113 (1978)
45. R. Kanya, Y. Morimoto, K. Yamanouchi, Phys. Rev. Lett. **105**, 123202 (2010)
46. R. Kanya, Y. Morimoto, K. Yamanouchi, Rev. Sci. Instrum. **82**, 123105 (2011)
47. B.A. deHarak, L. Ladino, K.B. MacAdam, N.L.S. Martin, Phys. Rev. A **83**, 022706 (2011)
48. J.C. Williamson, A.H. Zewail, Chem. Phys. Lett. **209**, 10 (1993)
49. F. Toffoletto, R.C.G. Leckey, J.D. Riley, Nucl. Instrum. Meth. Phys. Res. B **12**, 282 (1985)
50. R. Kanya, Y. Morimoto, K. Yamanouchi unpublished data
51. D.M. Bishop, Adv. Quantum Chem. **25**, 1 (1994)
52. K. Yamanouchi, M. Sugie, H. Takeo, C. Matsumura, K. Kuchitsu, J. Phys. Chem. **88**, 2315 (1984)
53. I. Hargittai, M. Hargittai (eds.), *Stereochemical Applications of Gas-Phase Electron Diffraction, Part A* (Wiley, New York, 1988)
54. K. Yamanouchi, *Quantum Mechanics of Molecular Structures* (Springer, Heidelberg, 2012)
55. R. Srinivasan, V.A. Lobastov, C. Ruan, A.H. Zewail, Helv. Chim. Acta **86**, 1761 (2003)
56. H. Ihee, V.A. Lobastov, U.M. Gomez, B.M. Goodson, R. Srinivasan, C.Y. Ruan, A.H. Zewail, Science **291**, 458 (2001)
57. R. Kanya, Y. Morimoto, K. Yamanouchi, Laser-assisted electron scattering and its application to laser-assisted electron diffraction of molecules in femtosecond intense laser fields, in *Multiphoton Processes and Attosecond Physics*, ed. by K. Yamanouchi, K. Midorikawa (Springer, Berlin, 2012), p. 351
58. F. Röser, D. Schimpf, O. Schmidt, B. Ortaç, K. Rademaker, J. Limpert, A. Tünnermann, Opt. Lett. **32**, 2230 (2007)
59. J. Limpert, F. Röser, T. Schreiber, A. Tünnermann, IEEE J. Sel. Top. Quantum Electron. **12**, 233 (2006)
60. J. Limpert, F. Röser, D.N. Schimpf, E. Seise, T. Eidam, S. Hädrich, J. Rothhardt, C.J. Misas, A. Tünnermann, IEEE J. Sel. Top. Quantum Electron. **15**, 159 (2009)
61. C.R.E. Baer, O.H. Heckl, C.J. Saraceno, C. Schriber, C. Kränkel, T. Südmeyer, U. Keller, Opt. Express **20**, 7054 (2012)
62. K.A. Kouzakov, Y.V. Popov, M. Takahashi, Phys. Rev. A **82**, 023410 (2010)

http://www.springer.com/978-3-319-00520-1

Progress in Ultrafast Intense Laser Science
Volume X
Yamanouchi, K.; Paulus, G.G.; Mathur, D. (Eds.)
2014, XIII, 156 p. 66 illus., 39 illus. in color., Hardcover
ISBN: 978-3-319-00520-1